Nuclear Instruments and Methods in Physics Research A 338 (1994) 336–347
North-Holland

NUCLEAR
INSTRUMENTS
& METHODS
IN PHYSICS
RESEARCH
Section A

Energy dependence of hadronic activity

T.A. Gabriel [a], D.E. Groom [b], P.K. Job [c], N.V. Mokhov [d,e] and G.R. Stevenson [f]

[a] *Oak Ridge National Laboratory, Oak Ridge, TN 37831-6356, USA*
[b] *Lawrence Berkeley Laboratory, Berkeley, CA 94720, USA*
[c] *Argonne National Laboratory, Argonne, IL 60439-4815, USA*
[d] *IHEP, Protvino, Moscow Region, Russian Federation*
[e] *SSC Laboratory, Dallas, TX 75237-3946, USA*
[f] *CERN, CH-1211 Geneva 23, Switzerland*

(Received 20 September 1993)

Two features of high-energy hadronic cascades have long been known to shielding specialists: a) in a high-energy hadronic cascade in a given material (incident $E \gtrsim 10$ GeV), the relative abundance and spectrum of each hadronic species responsible for most of the energy deposition is independent of the energy or species of the incident hadron, and b) because π^0 production bleeds off more and more energy into the electromagnetic sector as the energy of the incident hadron increases, the absolute level of this low-energy hadronic activity ($E \lesssim 1$ GeV) rises less rapidly than the incident energy, and in fact rises very nearly as a power of the incident energy. Both features are of great importance in hadron calorimetry, where it is the "universal spectrum" which makes possible the definition of an intrinsic e/h, and the increasing fraction of the energy going into π^0's which leads to the energy dependence of e/π. We present evidence for the "universal spectrum," and use an induction argument and simulation results to demonstrate that the low-energy activity scales as E^m, with $0.80 \lesssim m \lesssim 0.85$. The hadronic activity produced by incident pions is 15–20% less than that initiated by protons.

1. Introduction

The defining process in a high-energy hadronic cascade is the transfer of energy from the hadronic to electromagnetic sectors via π^0 production. The process is a "one-way street" in the sense that few hadrons are produced in electromagnetic cascades, while nearly 1/3 of the energy is transferred to the electromagnetic sector in each high-energy hadronic collision. This logic flow is shown in Fig. 1, where F_{π^0} is defined as the energy fraction transferred to π^0's in *all* cascade generations. We will later use f_{π^0} for the average energy fraction carried by the π^0's in a single interaction.

The number of secondaries increases very rapidly as the cascade evolves. The cascade continues until the final particles lose their energy by such processes as ionization, nuclear excitation, spallation, and fission. Ionization and spallation losses by high-energy particles contribute only negligibly to the total energy deposition, and it is fair to say that essentially all of the energy deposition, activation, neutron yield, etc., is produced by low-energy particles. For this reason the hadronic activity has very little memory of its origins, apart from an overall activity level.

For simplicity, we assume that the cascades are completely contained in a uniform medium. By "completely contained" we mean that there is no hadronic leakage except for front-face albedo loss. By "uniform" we mean "uniform over a neutron mean free path." Examples include concrete blocks, soil, and calorimeters consisting of alternating layers of absorber and readout material.

After defining the "hadronic sector" more carefully, we shall examine the extent to which the relative abundance and spectrum of each hadronic species are independent of the origin of the cascade, and then explore the energy dependence of F_h. Both have important ramifications for shielding, radiation levels, and calorimetry.

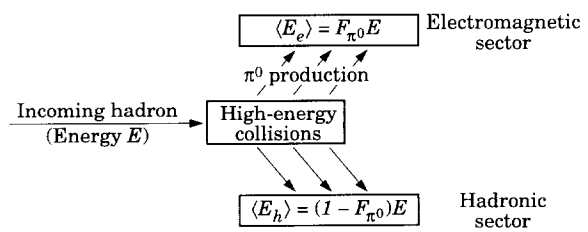

Fig. 1. Logic flow in a hadronic cascade. The energy in the hadronic sector is defined as the energy not going into π^0 production, although a more detailed treatment would exclude energy escaping from the front face of the absorber. Total containment of hadrons is otherwise assumed.

2. The hadronic sector

We have chosen to define the hadronic sector as containing all of the energy not carried by π^0's (plus possibly a few direct gamma rays, η's, and photons and electrons from high-energy radiative processes); that is, $F_h \equiv 1 - F_{\pi 0}$. It includes energy lost through ionization by high-energy hadrons, nuclear binding, the energy of heavy spallation fragments, and the energy of escaped neutrinos and muons. It also includes excitation gamma rays and electromagnetic energy released in nuclear processes such as (n, γ) reactions.

Our assignment of nuclear gamma rays to the hadronic sector is both arbitrary and convenient. We show later that the fraction of the hadronic energy carried by these photons scales with incident energy in the same way as other components, so that their inclusion causes no logical problem. The net effect of moving them from one sector to another is to slightly change F_h, and, for a calorimeter, to slightly change h, but there are practical advantages to including them with the hadronic sector. The π^0 energy fraction is easily and quickly calculated using just the high-energy part of the simulation code; indeed, there is no reason to run the calculation below the π^0 threshold. If the nuclear gamma ray contribution is also required, the complexity and running time are vastly exacerbated and agreement between codes is less likely.

Neutrino and high-energy muon losses are inevitable. For example, about 1% of the hadronic energy goes into the neutrinos via the π^+–μ^+–e^+ decay chain. These losses also scale with the rest of the hadronic energy and are properly part of the hadronic sector, even though the energy never appears on a radiation monitor or calorimeter readout.

The front-face albedo losses are also included. In a 50 GeV cascade, they typically carry of order 1% of the energy, and the fraction falls rapidly with energy [1]. Their contribution is small enough to ignore for our present purposes, but they should be included as a third sector in a more detailed treatment.

3. The universal low-energy hadron spectrum

A small number of high-energy secondary particles (mostly pions) and spallation products are produced in the first collision of a high-energy primary hadron incident on a calorimeter or other beam stop. The secondary π^0's decay, and the other high-energy hadrons undergo subsequent inelastic collisions. The number of interactions ("stars") increases rapidly as the particle energy degrades. Most of the hadronic activity, and in fact most of the energy deposition, occurs at low energies. In describing low-energy hadronic activity, we technically mean hadronic activity below the π^0 production threshold, but for practical purposes it matters very little if the cutoff is at 0.1 or 1 GeV.

Although the level of activity varies with the energy of the incident hadron, the energy distribution and relative importance of each hadronic species is independent of incident species or energy. Two effects seem to combine to produce this result: a) the secondary particle spectrum and inelastic cross section in a given high-energy collision in the cascade are relatively independent of the energy of the colliding particle, so that any collision is very much like any other; and b) the number of generations is fairly large, so that there is little memory of the original incident hadron. Even leading-hadron effects tend to be lost within the first 2–5 collisions, as will be discussed later.

This "universal spectrum" concept has been familiar to radiation shielding experts for more than two decades. Previous work on the subject will be documented in section 9. In this section we illustrate the concept with simulations using modern code.

The results of a MARS10 [2] simulation are shown in Figs. 2 and 3[#1]. Fig. 2 shows neutron spectra (averaged over the cascade) produced by 10, 100, and 1000 GeV protons striking solid lead, all normalized for relative agreement at low energies. Almost all of

[#1] The quantity $d\phi/d\ln E = E\, d\phi/dE$ is called the *lethargy spectrum* by radiation physicists, but it is widely used to describe such quantities as differential cross sections when a logarithmic scale on the horizontal axis is used. It has the advantage that if the vertical scale is linear, the area under the curve is the integral of $d\phi/dE$.

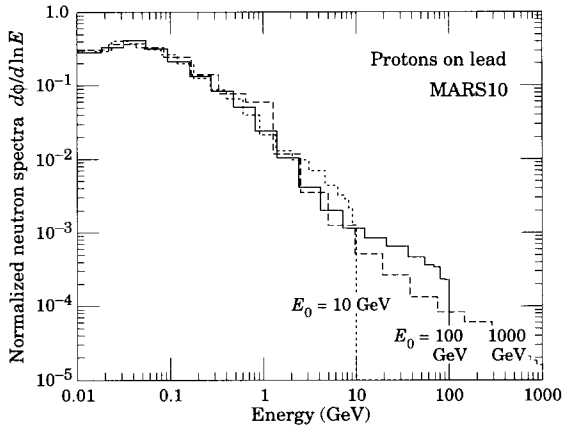

Fig. 2. MARS10 simulations of the neutron spectra in a lead beam stop for incident proton energies of 10, 100, and 1000 GeV. Spectra are for all of the neutrons in the cascade. They are normalized for relative agreement at low energies to emphasize the shape similarity below the beam energy cutoff.

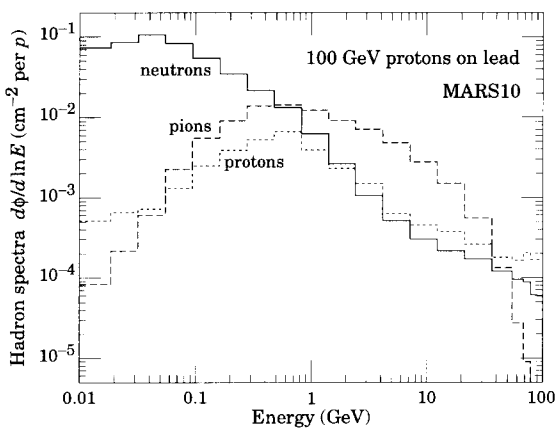

Fig. 3. MARS10 simulations of the neutron, proton, and pion spectra for 100 GeV incident protons on lead. At low energies the charged particles are removed by ionization loss. At high energies the neutrons and protons have similar spectra. The relative numbers, particularly of neutrons, will be different in a different material.

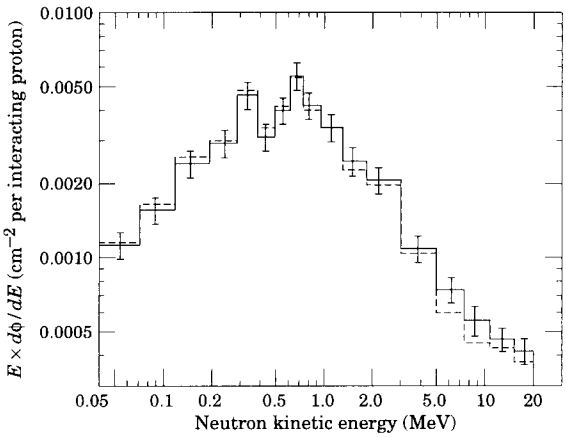

Fig. 4. Neutron spectra at 875 GeV and 20 TeV in the Tevatron tunnel. The solid histogram is an HETC/MORSE simulation at 875 GeV, and the dashed histogram is a simulation at 20 TeV, normalized to emphasize the identity of the spectral shapes.

the particles have energies below 1 GeV, even for a 1 TeV incident beam, and the shapes of the spectra (below cutoffs set by the incident beam energies) are identical within the accuracies of the simulations. There may be some excess in the decade just below the cutoff energy.

Fig. 3 shows spectra for the three main hadronic species, this time for an incident proton energy of 100 GeV. As might be expected, the high-energy proton spectrum is about the same as that of neutrons. At low energies the protons quickly lose energy by ionization. They are nearly two orders of magnitude less important than neutrons at 100 MeV and vanish rapidly as the energy decreases. Charged pions have a similar behavior, but they are more abundant than nucleons at high energies.

When transport is extended to lower energies, the neutron lethargy spectrum shows a broad "evaporation peak" with its maximum just below 1 MeV [3]. For example, Fig. 4 shows HETC88 simulations of the neutron flux at 0.875 TeV and 20 TeV produced by beam-gas collisions in the Tevatron tunnel [4–6]. The 20 TeV flux has been scaled downward for comparison of the spectral shapes. Experimental measurements of the neutron spectrum at 900 GeV are in very good agreement with the simulation results.

In Fig. 5 we show the various fractional contributions to the hadronic energy as simulated with CALOR [7] for protons and negative pions incident on an iron cylinder. (The 10-GeV points are anomalous for code-dependent reasons.) To the extent that the mix of low-energy hadronic components is independent of energy, each component should be a constant. Some energy dependence is actually evident. For incident protons the fraction of the hadronic energy deposited by secondary charged pions increases from 15% to 19% between 20 and 500 GeV, in exchange for a decrease in the secondary proton energy deposit from 40% to 38%. The situation is similar for incident pions, but in this case there are comparatively more pions and fewer protons. As can be

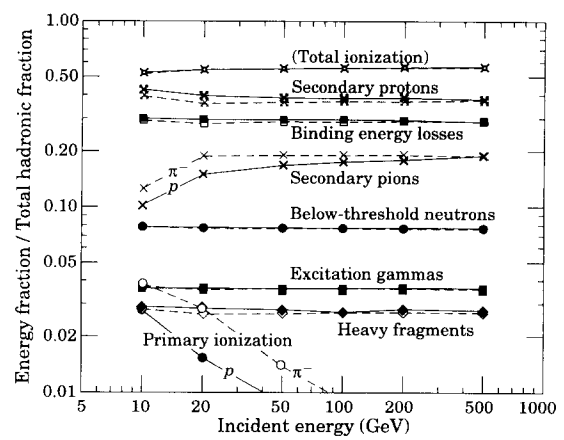

Fig. 5. Hadronic energy loss by various mechanisms in cascades initiated by protons (solid lines) and negative pions (dashed lines) in iron, as simulated with CALOR. Energy deposits are given as fractions of the energy not carried by π^0's. "Total ionization" is the sum of primary and secondary ionization by pions and protons, and is shown to demonstrate the constancy of the sum of all ionization contributions. Exclusive of this subtotal, the sum of the contributions at each energy is unity.

Table 1
CALOR89 simulation values for e and h for four calorimeter configurations. Each of the identical cells in each configuration consists of a 100 cm × 100 cm absorber plate as specified, followed by a 0.3 cm scintillator plate with the same transverse dimensions. In the two 2.54 cm plate configurations there are 68 cells. For the 1.90 cm configurations there are 92 cells in the lead case and 90 cells in the iron case. The arbitrary normalizations of e and h are chosen in this case relative to the sampling efficiency for minimum ionizing particles

E_{π^-} [GeV]	2.54 cm lead		1.90 cm lead		2.54 cm iron		1.90 cm iron	
	e	h	e	h	e	h	e	h
25	0.601	0.704	0.603	0.674	0.852	0.578	0.854	0.555
50	0.602	0.708	0.605	0.670	0.850	0.576	0.858	0.552
100	0.599	0.703	0.605	0.677	0.851	0.563	0.858	0.559
150	0.603	0.703	0.603	0.677	0.855	0.561	0.857	0.545
227	0.602	0.703	0.605	0.678	0.857	0.569	0.855	0.543
Average	0.601	0.704	0.604	0.675	0.853	0.569	0.856	0.551

seen from the top curve, the sum of all the ionization energy deposited by pions and protons is virtually constant and independent of both species and energy.

In hadron calorimetry, the sampling efficiencies are in general different for the electromagnetic and hadronic components of the deposited energy. These efficiencies (e and h, respectively),[#2] as obtained from CALOR89 simulations, are given in Table 1 for four uniform calorimeter configurations with incident π^- energies ranging from 25 to 227 GeV. The constancy of h for each configuration provides further evidence for the energy independence of the hadronic spectra. Since e is also constant (calorimeters normally have linear response to electrons), the ratio e/h is also constant. If it were not for the "universal spectrum," an intrinsic e/h could not be defined.

Of course the "universal spectrum" theorem is not quite true. We have already discussed the change in the proton/pion ratio shown in Fig. 5. A higher-energy primary is capable of producing more high-energy secondaries, but these contribute little to the total energy deposition. Moreover, there are a variety of geometrical effects. The higher-energy secondaries and spallation nucleons tend to concentrate nearer the axis and nearer the beginning of the cascade. Only neutrons propagate to large radial distance from the shower core, and low-energy neutrons (below ~150 MeV) have a flatter radial distribution than do higher-energy components [9]. Such effects could be important in some situations, such as activation near the cylindrical surface of a beam stop. However, in situations ranging from shielding to calorimetry, there is a certain amount of averaging over the cascade geometry, and the spatial variations tend to average out.

[#2] Although it is the ratio of e and h which is usually encountered, it is useful to refer these sampling fractions to the sampling fraction of the active medium for a minimum-ionizing particle [8]. For example, suppose an ensemble of minimum-ionizing particles lose 100 GeV in the "2.54 cm Lead" calorimeter of Table 1. Since $e = 0.60$, we would expect a signal only 0.60 as large from the cascade of a 100 GeV photon. In both cases, only a small fraction of the energy is actually deposited in the readout layers, which in this case is plastic scintillator.

4. Measures of low-energy hadronic activity

There are many measures of the low-energy hadronic activity discussed in the previous section, all of which exhibit about the same dependence on incident hadron energy. These include:

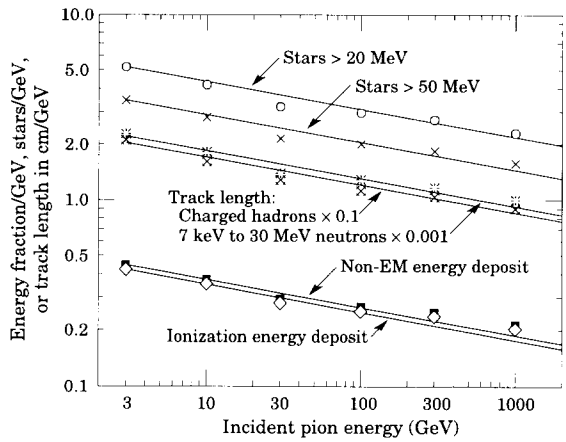

Fig. 6. Measures of hadronic activity simulated with FLUKA92 [10] for protons incident on an iron cylinder. Of particular importance is the number of nuclear interactions (stars) produced by hadrons with energy above some cutoff, here 20 MeV and 50 MeV, which can be related to radionuclide production. The solid lines have a slope of −0.15.

(i) Number of nuclear interactions ("stars") produced in the absorber by hadrons whose energy exceeds some threshold E_{th}. Most such interactions are induced by hadrons (usually neutrons) with energies not far above E_{th}, and the comparatively few interactions with $E > E_{th}$ contribute little to the total. This measure has the advantage of being easily tallied by the transport code, and it is readily available. This and other code-produced quantities are shown in Fig. 6; other examples are shown in Fig. 5.

(ii) The yield of a given radionuclide; e.g. ^{54}Mn in an iron absorber, ^{60}Co in stainless steel, or ^{239}Np in a uranium calorimeter [11]. The proportionality of activation to star density is often exploited in estimating radioactivation [12,13].

(iii) The hadronic part of calorimeter response. The total response is a combination of electromagnetic response (to the π^0 decay photons) and response to the predominately low-energy hadronic activity, but these can be separated by analyzing the energy dependence of the calorimeter's response to incident hadrons.

In summary: Any measure of hadronic activity is about as good as any other, as long as one samples the entire cascade. The flux of side-leakage neutrons in a calorimeter provides a measure of hadronic activity, as does the total activation. However, the relative importance of various measures is different in different materials.

5. Heuristic derivation of energy dependence

A simple induction argument may be used to obtain the energy dependence of the low-energy hadronic activity. Let $N(E)$ be one of the measures of this activity discussed above; to fix ideas let it be the average number of nuclear stars produced by cascade particles with energies above E_{th} in a cascade initiated by a hadron with energy E (the hadron may already be a secondary in a larger cascade). Now consider the activity $N(nE)$ produced by a hadron with energy nE, where n is a multiplier roughly identified with the average multiplicity of high-energy secondaries (charged and neutral) produced in its first collision. Unless it is a π^0, a secondary with energy E_i produces hadronic activity $N(E_i)$, and

$$N(nE) = \sum_{\text{daughters}(\neq\pi^0)} N(E_i)\,, \tag{1}$$

where the sum is over secondary particles exclusive of π^0's. Now let us replace the correct sum of hadronic activity contributions with the available energy fraction times an average contribution:

$$N(nE) \approx (1 - f_{\pi^0})\, n\, N(E)\,. \tag{2}$$

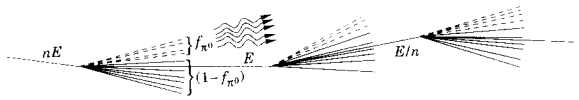

Fig. 7. Schematic of cascade. It is assumed that in each generation the average energy of the cascade particles decreases by a factor n and that an average fraction f_{π^0} of the energy leaves the hadronic sector via π^0 production.

Here a fraction of the energy f_{π^0} is lost to the hadronic sector through π^0 production. (We distinguish f_{π^0}, the fraction of the energy going into π^0's in one collision, from F_{π^0}, the energy fraction going into π^0's in all the generations of the cascade.) The cascade process as we are modeling it here is shown schematically in Fig. 7.

Insofar as n and f_{π^0} can be treated as constants, the solution to this iterative equation is a power law,

$$N(E) = K E^m\,, \tag{3}$$

with

$$1 - m = \frac{\ln\left(1/(1 - f_{\pi^0})\right)}{\ln n}\,. \tag{4}$$

The other assumptions can be discussed most easily after examining the range of the variables.

If only pions were produced, then we would have $f_{\pi^0} = 1/3$. Nucleons carrying a substantial energy fraction are also produced by a variety of processes, so this value should only be taken as an upper limit. The Monte Carlo simulations suggest values closer to 1/4.

Charged multiplicities in the relevant energy range are in the range 6–7 [14], so the total multiplicity should be about 10. On the other hand, secondaries with energies below the pion-production threshold do not continue the cascade process described above. A number about half this size thus appears to be relevant.

For $f_{\pi^0} = 1/4$ and $n = 5$, we find $m = 0.82$. If f_{π^0} is increased to 1/3, then m decreases to 0.75. For $n = 10$ and $f_{\pi^0} = 1/4$, $m = 0.87$. Contours of fixed m are shown as functions of n and f_{π^0} in Fig. 8.

Eq. (2) was obtained by assuming that the sum of activities produced by k ($\approx (1 - f_{\pi^0})n$) particles with different energies E_i could be replaced by k times the hadronic activity produced by one particle with the average energy $E = (\sum_1^k E_i)/k$. Making use of the power-law solution, we see that this is equivalent to

$$\sum_{i=1}^{k} E_i^m \approx k E^m\,. \tag{5}$$

However, if only one of the secondary particles carried all of the non-electromagnetic energy, the left side would be $k^m E^m$, which is smaller than the right side by a factor k^{m-1}. If j particles ($j \leq k$) divided the en-

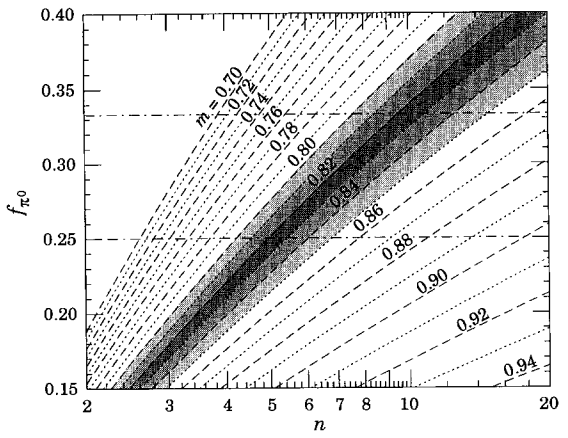

Fig. 8. The average fraction of the energy entering the electromagnetic sector f_{π^0} as a function of the average total multiplicity n for a single high-energy collision in a cascade for fixed values of the power m, as given by Eq. (4). One expects $f_{\pi^0} \approx 1/4$ and, with more uncertainty, $n \gtrsim 5$. Estimates of m from the most dependable simulations fall in the shaded region.

ergy equally, then the factor would be $(k/j)^{m-1}$. With $n \approx 5$, the result would be about 20% smaller if only one particle carried all the energy, and 10% smaller if two particles divided the energy equally. In a naïve spectator model, a leading hadron tends to carry off about half of the energy. The fragmentation functions favor very unequal energy division among the remaining cascade particles. As a result, our equal-energy assumption probably overestimates the quantity on the right side of Eq. (1) by 10–20%—if we strictly interpret n as the total multiplicity. In reality, the net effect of our approximation is to reduce the multiplier n by 10–20%. It should be thought of as an energy scale factor between generations rather than as a cascade particle multiplicity.

The remaining issues concern the effect of the energy dependence of n and f_{π^0}, which were implicitly assumed to be constant in the above development. The insensitivity of m to either variable is evident from the above discussion or from Fig. 8. The multiplicity increases only logarithmically with energy, so $\ln n$ varies extremely slowly. Presently available data show no conclusive evidence for the increase. Similarly, $\ln(1 - f_{\pi^0})$ is insensitive to changes in f_{π^0} over its expected range.

Finally, we have assumed that the products of a collision will themselves induce similar collisions. This assumption will break down when the secondaries have energies below the π^0 production threshold. The minimum incident energy for the validity of our argument should thus be about 10 GeV. In any case, mass effects become important at lower energies.

It is useful to rephrase the logic: After each collision in a hadronic cascade, only $(1 - f_{\pi^0})$ of the energy is available (on the average) for the next generation. This factor is applied every time the energy increases by the multiplicity, which results in a power-law increase in low-energy activity with increasing energy of the incident hadron. Stated differently, every collision is very much like every other collision except for the energy scale. The very nature of the process leads to a power-law-like behavior.

According to Eq. (3), the level of low-energy hadronic activity is *proportional* to E^m. We can fix the proportionality constant by a dimensional argument:

$$E_h = E_0(E/E_0)^m = E(E/E_0)^{m-1} . \quad (6)$$

The average hadronic energy fraction F_h in a collision is E_h/E, or

$$F_h \equiv (1 - F_{\pi^0}) = (E/E_0)^{m-1} . \quad (7)$$

Here E_0 is introduced as a scale energy. As can be seen from Eq. (7), it is the extrapolated energy at which the cascade is entirely hadronic, or an effective turn-on energy for π^0 production. In practice F_h must fall below the power-law extrapolation at a somewhat higher energy, and should reach unity at the π^0 threshold. This situation is shown in Fig. 9, where the points are from a CALOR simulation for protons incident on tin. In this case the extrapolated intercept is at E_0 = 3.2 GeV, and the dotted line with the question mark indicates the trend of the expected behavior.

Understanding E_0 as an effective π^0 cutoff energy provides yet another way to obtain our expression for

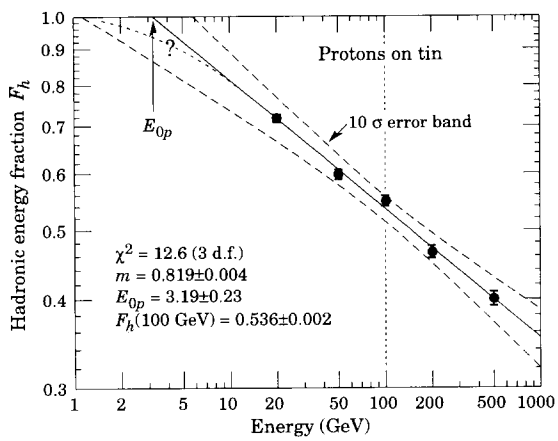

Fig. 9. An example of the fitting procedure used for the CALOR run sequence. Point errors in F_h are taken as $0.13/\sqrt{N}$ [15], where in this case N = 200 histories for each point. The error band is enlarged to $\pm 10\sigma$ for visibility. Although the value of E_0 is highly correlated with the slope m, F_h(100 GeV) is uncorrelated and has the minimal error.

m. The previous cascade generation was induced by hadrons with average energy nE_0, etc., so if there were n_g generations, $E = n^{n_g}E_0$, or $E/E_0 = n^{n_g}$. In each generation, F_h is reduced by the factor $(1 - f_{\pi^0})$, so

$$F_h = (1 - f_{\pi^0})^{n_g} = n^{(m-1)n_g} . \quad (8)$$

From the relationship $(1 - f_{\pi^0}) = n^{(m-1)}$ one immediately recovers Eq. (4).

6. Comparison with Monte Carlo simulation results

Simulations using MARS [2], CALOR [7], and FLUKA [17] have been use to examine the functional form of $F_h(E)$, and, given that a power-law description is adequate, to find the parameters m and E_0.

The energy dependence for a number of measures of hadronic activity was investigated with all three codes prior to 1989. The results were similar to those shown in Fig. 6. On this basis, it was concluded that power laws with $m \approx 0.85$ provided a good description of all the high-energy data. The intercept E_0 was not studied, but it was thought that $E_0 \approx 1$ GeV [16].

A series of FLUKA runs was used to investigate the details of the distribution of the electromagnetic energy fraction on an event-by-event basis in a solid lead beam stop [15]. The behavior of the first moment of the distribution, plotted as $1 - F_{\pi^0}$, is shown in Fig. 10. A least-squares fit of Eq. (7) yields $m = 0.87$ and $E_0 = 0.76$ GeV. There is some evidence for decreasing slope, as might be expected from the slow increase of multiplicity with energy, but this is not corroborated by our other studies.

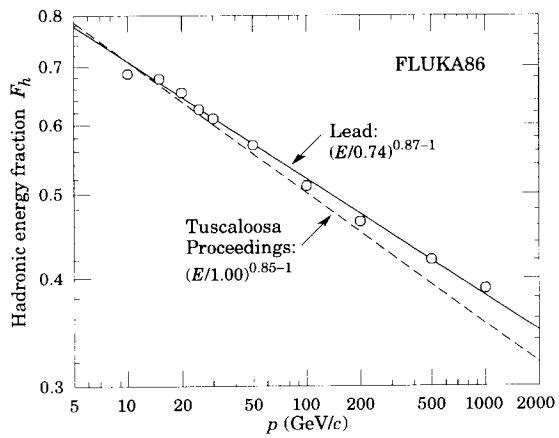

Fig. 10. The mean hadronic fraction F_h as simulated with FLUKA86 for negative pions incident on a lead target. The least squares fit of the function $(E/E_0)^{m-1}$ yields $m = 0.87$ and $E_0 = 0.74$ GeV, shown by the solid curve. The dashed curve is from a preliminary report, assuming $m = 0.85$ and $E_0 = 1.0$ GeV [16].

A similar analysis was made using CALOR89 simulations for a test-beam calorimeter with incident pions, for which e and h are reported in Table 1. This time the best-fit power is somewhat smaller, about 0.83 for both lead and iron. The difference seems to reflect π^0 production differences between the two codes. In the lead case $E_0 = 1.3$ GeV, and for iron it is 0.7 GeV, reflecting 5% less hadronic activity (fewer neutrons) in iron than in lead.

An estimate of the exponent at higher energies can be obtained from HETC/MORSE comparisons of the expected neutron flux at the Tevatron and SSC, which were run at 20 TeV and 875 GeV [4]. The ratio of longitudinally integrated neutron fluxes was 14.0 for the direct flux and 13.7 with the inclusion of albedo flux, corresponding to $m = 0.84$ in both cases. This is in good agreement with the lower-energy HETC results, and argues that m does not change much with increasing energy.

The above simulations were made with a wide variety of codes, code versions, incident particles, absorber materials, and energy ranges. While they validate the power-law functional form for F_h, the values of the slope and (particularly) the intercept scatter widely. Accordingly, a detailed series of CALOR runs was made to study:

(i) The dependence of m and E_0 on the atomic number of the absorber. In hadron collisions with higher-Z nuclei, one might expect a larger fraction to go into lower-energy secondaries (more neutrons are produced in lead than in iron). The decrease in the amount of energy going into π^0's might be reflected in a small increase in m and/or an increase in E_0.

(ii) The dependence of m and E_0 on the incident particle species. Much of the energy in a given pion(nucleon)–nucleus collision is carried by a leading pion (nucleon). There is some probability of charge exchange, which in the pion case removes the energy from the hadronic sector. As it turns out, the effect is significant.

Most of the runs were for incident π^-'s or protons at either four or five energies on aluminum, iron, tin, and lead. Two hundred histories were usually followed, which in principle should determine F_h with a statistical error of slightly less than 0.01 [15]. In some cases π^+'s and neutrons (the other possibilities permitted by CALOR) were run, as were protons on concrete. Least-squares fits to power laws were obtained for each energy sequence.

The results for an iron beam stop are shown in Fig. 11. As can be seen, the results for protons and neutrons are not distinguishable, nor are the results for positive and negative pions. For simplicity, the fit results are shown only for π^- and p.

Typically, the pion results at 10 GeV are high as compared with power-law extrapolations from higher

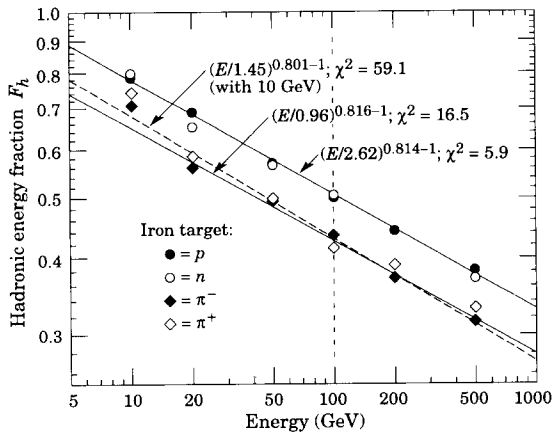

Fig. 11. Hadronic fractions for incident $\pi^{\pm}$, p, and n on an iron target, as simulated by CALOR. The straight lines are power-law fits to the proton and π^- data. For pions in heavy materials the 10 GeV case is aberrant because of the way intranuclear cascades are handled. The dotted curve includes this point, and the solid curve excludes it. In general, acceptable fits are obtained for all materials and energies for incident protons, and for all materials and energies above 10 GeV for pions.

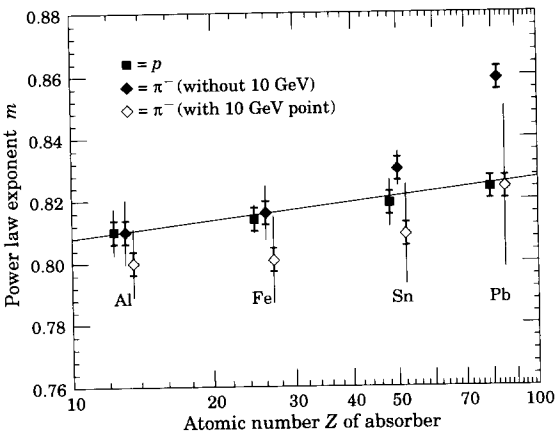

Fig. 12. Values of m for fits to the hadronic energy fraction of the form $(E/E_0)^{m-1}$. Errors with flags are statistical only, and errors without flags are scaled by the square root of the reduced χ^2 per degree of freedom. Points are plotted to the right or left of the correct atomic number Z for clarity. The straight line is only a guide for the eye.

energies. This is thought to be an artifact of CALOR; it is not seen in preliminary results obtained with FLUKA and MARS. The effect grows with Z, the atomic number of the absorber. χ^2 increases from 34 to 199 (with 3 d.f.) in going from aluminum to lead when the 10 GeV point is included. The proton results including the 10 GeV runs and the pion results above 10 GeV give acceptable power-law fits. No trends away from power-law behavior are seen. A bad χ^2 usually reflects random scatter in excess of the expected variance.

Results for the slope m are shown in Fig. 12. The error bars with flags include statistical errors only. The thin bars without flags have been scaled by the square root of the reduced χ^2 to include, in part, the badness of the fitting function and/or data, in this case the 10 GeV problem mentioned above. The high point for π^- on lead is not corroborated by the test-beam calorimeter runs with the same code. For the "Lead 1" and "Lead 2" cases reported in Table 1, we obtain $m = 0.832$ and $m = 0.842$, respectively. We conclude that a) there is no evidence for π/p slope difference beyond the code uncertainties, and b) there is weak evidence for a gradual increase of m with Z. This would indicate a smaller π^0 energy fraction with increasing Z, as might be expected from the above discussion.

Since E_0 is an extrapolated intercept, it is highly correlated with the slope m. Given the energy range of the simulations (which are about the same as for test beam runs), the "fulcrum" of the fits is at about 100 GeV. At this energy the correlation between slope and hadronic fraction vanishes. For this reason we use $F_h(100\ \text{GeV})$ as a measure of the hadronic activity. Fig. 9 illustrates the situation. The error band on F_h is exaggerated by a factor of ten for visibility. As can be seen, the error in F_h is minimal at 100 GeV.

$F_h(100\ \text{GeV})$ is shown in Fig. 13. The statistical errors are in all cases smaller than the points. The scaled statistical error is larger than the point only for the infamous π^- on lead case when all energies are

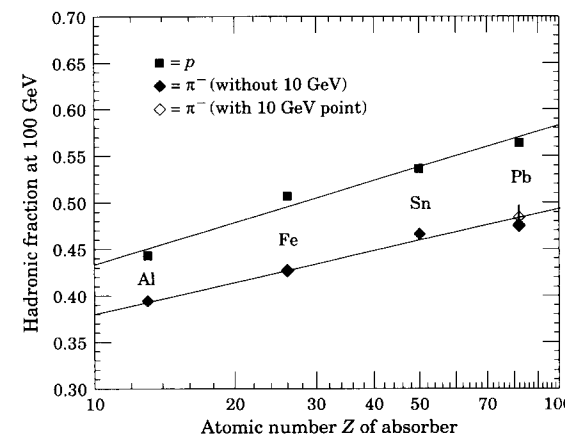

Fig. 13. Values of the quantity $F_h(100\ \text{GeV})$ for fits to the hadronic energy fraction of the form $F_h(E) = (E/E_0)^{m-1}$. This quantity rather than E_0 is used because it is nearly uncorrelated with the slope m. The straight lines are guides for the eye, not fits.

included. We conclude that a) the hadronic fraction increases with Z (as might have been expected—it is easier to produce neutrons from lead than from iron), and b) there is about 15% less hadronic yield from pions than from protons, with the difference increasing slightly with Z. The data shown in Fig. 11 indicate that there is no sensible distinction between incident protons and neutrons, nor between positive and negative pions.

7. Pion–proton response difference

The difference in the hadronic activity produced by pions and protons or neutrons may be understood in fairly simple terms. To the extent that the hadron-nucleus collision may be described as the collision between two constituent quarks, the remaining quark (in the case of a pion) or quarks (in the case of a nucleon) from the projectile carry 1/2 or 2/3 of the incident energy and emerge as leading hadrons after picking up another quark from the sea. Kinematic effects and further collisions modify the result, but a leading pion or nucleon, depending upon the kind of incident particle, emerges with a large fraction of the initial energy.

If the incident particle is a proton, it matters very little for cascade development whether the leading hadron is a proton or a neutron. However, if a charged pion is incident a π^0 can emerge, removing energy from the hadronic sector. The size of the effect can be approximately bracketed as follows:

Suppose that all charges are equally probable for the leading pion. In this case an average of 1/3 of the leading-pion energy enters the electromagnetic sector, and, for a leading hadron carrying 1/2 of the incident energy, 1/6 of the incident energy is lost to hadronic activity. This is easily summed over subsequent generations, and one finds that 1/4 of the energy is lost by leading-pion charge exchange. The result is quite sensitive to the assumed average energy fraction carried by leading pion.

Charge equilibrium probably represents an upper limiting case. At the other extreme, one might use data for the reaction $\pi^- + \mathrm{p} \rightarrow \pi + X$ to set a lower limit, since in this case further charge exchange in an extended nucleus cannot occur. Pauss et al. have measured inclusive spectra in the forward fragmentation region [18], and find that 19% of the pions with 50% of the incident energy are neutral. The fraction drops to 14% for leading pions with 80% of the incident energy. Charge exchange is improbable when very little energy is lost by the leading pion, but in this case the collision does not contribute much to cascade development. These fractions are about half the size of those given in the equilibrium argument above, so that if they are typical we might expect 1/8 of the hadronic energy to be removed by leading pion charge exchange.

In spite of their sensitivity to the leading-hadron energy fraction, these estimates show that the CALOR results are physically reasonable. One cannot speak just of the hadronic fraction F_h, but must distinguish F_π and F_p. The lower hadronic yield from pions has the interesting consequence that protons produce a smaller signal than pions of the same energy in a non-compensating calorimeter[#3].

In the above, we have concluded that F_π/F_p is about 0.85, depending somewhat on material but not on energy; that is, m is the same for pions and nucleons. Is this really true? Our conjecture is that this is so, in spite of the fact that the codes sometimes yield the opposite result. In particular, the CALOR runs yielding the large difference in m for lead, as shown in Fig. 12, imply that the curves for F_π and F_p cross at several TeV. At least some versions of FLUKA show the same effect at lower energies. Physically, the larger m (flatter F_h curve) means that incident pions underproduce π^0's as compared with incident nucleons.

In the first place, the pion/nucleon difference must disappear within 2–5 generations, depending on the average energy of the leading pion. If this energy is half the primary energy, then after three generations the leading pion has an energy comparable to the non-leading secondaries in the first collision. The distinction between incident pions and nucleons is lost for the rest of the cascade.

Secondly, one of these early leading pions can always charge exchange, so that on the average a pion of any energy produces less hadronic activity than does a nucleon. The curves cannot cross. It is difficult to find any significant energy dependence for the charge exchange probability, so that we would expect a very nearly energy-independent F_π/F_p. This implies parallel curves for the two cases when $\ln F_h$ is plotted as a function of $\ln E$, as is done in Fig. 11. To very nearly the degree to which m is a constant, it is the same for pions and nucleons.

8. Proposed experimental measurements

The results shown in figs. 12 and 13 were obtained with CALOR, which uses the same high-energy production model as FLUKA. There are unanswered questions, ranging from the values of the slopes and relative values of F_h(100 GeV) to the extent to which the power law description is valid. For example: Is

[#3] A moderately non-compensating calorimeter should show a π/p ratio measurably different from unity [19].

Table 2
Hadronic fractions predicted by CALOR as a function of absorber material and incident hadron species, scaled to 1.00 for protons on lead. The relative fractions are evaluated at 100 GeV using the data shown in Fig. 13, but are independent of energy if m is the same for pions and protons

Material	p	π^-
Lead	1.00	0.84
Iron	0.90	0.76

the power law approximation to hadronic yield in lead really valid for both pions and protons over the available test beam energy range? Is m really the same for pions and protons in a given material, as argued above?

It does not appear difficult to answer these questions. One builds a "calorimeter" in which only the hadronic or electromagnetic activity is sampled. For example, dimensions are chosen to provide a small amount of side leakage, and the device is surrounded by neutron counters. Alternatively, it is a sampling calorimeter with Cherenkov readout, sensitive only to the electromagnetic sector.

The relative hadronic activities in iron and lead for incident pions and protons predicted by CALOR are shown in Table 2. For either iron or lead, the relative neutron yield for pions and protons gives the ratio $F_\pi(E)/F_p(E)$, and the neutron yield as a function of energy gives the functional form for F_h.

The comparison between iron and lead is more difficult. Not only is it difficult to ensure the same fractional leakage in both cases, but also the scaling between neutron flux (or any another measure of hadronic activity) and total hadronic activity will not be same for different substances. In this case the Cherenkov readout option is viable, but the construction and precision calibration of the device are much more complicated.

The mean for any one particle type and energy should be determined to 1–2%. In addition, it is very desirable to obtain sufficient statistics in any individual event to study the fluctuations in F_h. This distribution function determines the so-called "constant term" in calorimeter resolution. For pions the standard deviation of F_h is expected to be about 0.13, almost independently of energy [15]. A useful measurement of the response on an event-to-event basis would thus require detecting several hundred neutrons per event, which seems unlikely. From the above discussion of leading-pion charge exchange, one would expect a much narrower distribution in the case of incident protons.

9. Previous work

The idea that the low-energy particle distribution (the "universal spectrum") is independent of its origins probably dates to the work of Moyer, who in a 1957 conference used the cosmic-ray neutron spectrum as representative for accelerator shielding calculations [20,21]. O'Brien used the concept of a "universal production spectrum" in numerous papers, e.g. in ref. [22]. His spectrum, developed by Ranft and Borak, was based on work by Trilling. The universal spectrum of low-energy particles is a consequence of the nearly energy-independent production spectra and the forgetfulness resulting from many generations. A particularly explicit statement of the concept is given on page 39 of a book by Van Ginneken and Awschalom in 1975 [23]:

"It is well known from ORNL's and similar calculations and also from observation that for a sufficiently well developed cascade, the shape of the spectrum for the low energy particles is rather independent of location within the shield, incident energy or even shielding material (as long as the hydrogen content is essentially the same)... it is then sufficient to assume a representative shape for the lower end of the spectrum."

They go on to use the spectra given in Fig. 2 of ref. [24]. These spectra seem to have been widely adopted as representative, although the paper makes no mention of its applicability to other energies and situations.

Nor is the power-law growth of hadronic activity a new idea. In shielding discussions it is related to the source strength parameter in the Moyer model, which is related to multiplication in cascades. Thomas and Stevenson credit the power law to Lindenbaum [25], although it is not in the reference they cite [26]. Lindenbaum suggests $m \approx 0.5$. Thomas and Thomas use later studies to conclude $m = 0.80 \pm 0.10$ [27], and others have extended the range of applicability to higher energies [28,29]. In particular, Cossairt et al. used CASIM [30] to obtain $m = 0.84 \pm 0.02$ in iron, in agreement with absorbed dose measurements at 400 and 800 GeV. In any event, these discussions did not go beyond the confines of the Moyer model, and Thomas and Stevenson assume elsewhere in the same reference that neutron yield is proportional to incident energy in order to ensure an overestimate of hazard.

In a 1972 paper, O'Brien noted that the number of stars divided by the incident energy could not be constant, but must decrease with increasing energy [31]. The curve in his Fig. 1 corresponds to $m = 0.84$, and would have been recognized as a power law had he used a logarithmic vertical axis. The lack of energy dependence in the Monte Carlo data shown in the figure reflects insufficient π^0 production in the early trans-

port codes. O'Brien was aware of the Moyer model work at Lawrence Berkeley Laboratory, but evidently no paper was published supporting the assertion that neutron production, for example, grew as a power of the incident energy [32].

10. Discussion

We have made two points: a) the concept of low-energy hadronic activity with little memory of its origins is fundamental to studies of shielding, radioactivation, and calorimeter response, and b) the very nature of the cascade process is such that the level of the hadronic activity scales very nearly as a power of the incident energy, that is, any measure of the activity is proportional to E^m.

The exponent m seems to lie in the range 0.80 to 0.85, depending on the Monte Carlo code used to study it and not depending strongly on the material in which the cascade occurs. Since every collision is very much like every other collision, it is possible to obtain an estimate of the exponent by means of an induction argument. The exponent is a function of the average π^0 energy fraction and multiplicity of high-energy secondaries in a single hadron–nucleus collision.

The hadronic energy fraction in a cascade, defined as the energy not transferred to the electromagnetic sector by π^0 production, is given by $(E/E_0)^{m-1}$, where E_0 is the extrapolated energy at which the hadronic energy fraction would reach unity in the absence of deviations from power-law behavior at low energies. Qualitatively, E_0 is the energy at which π^0 production becomes important. It is larger for lead than for iron, reflecting the fact that at a given incident energy a larger fraction is lost to nuclear processes for heavier, less tightly bound nuclei. E_0 is appreciably larger for incident protons than for incident pions, evidently as a consequence of leading-hadron charge exchange.

At the moment there are differences in the results obtained from different codes and code versions, and some internal inconsistencies. Given the implications of these parameters for both radiation level studies and calorimetry, we view it as important to obtain test beam verification of the both the functional form and the parameters.

The asymptotic behavior of the hadronic fraction cannot be overemphasized. Since the exponent m is of necessity less than one, the hadronic fraction slowly approaches zero as the energy increases. This feature is well known in cosmic-ray physics, where the energy deposition in energetic air showers is predominantly electromagnetic. For calorimetry it means that the asymptotic response to a pion is the same as that for an electron: $e/\pi \rightarrow 1$, and the hadronic response is asymptotically linear.

Acknowledgements

Although we are indebted to many or even all of our coworkers for discussions of the codes and the ideas, we are particularly grateful for the hours of thoughtful discussions with F. S. Alsmiller, R. G. Alsmiller, Jr., A. Ferrari, T. Handler, K. O'Brien, F. E. Paige, and J. Ranft.

This work was supported in part by the management of CERN, and by the U. S. Department of Energy under contracts W-31-109-ENG-38 (Argonne National Laboratory), DE-AC03-76SF00098 (Lawrence Berkeley Laboratory), DE-AC05-840R21400 (Oak Ridge National Laboratory, managed by Martin Marietta Energy Systems, Inc.), and DE-AC35-89ER40486 (SSC Laboratory).

References

[1] D.E. Groom, in: Proc. 1990 DPF Summer Study on High Energy Physics Research Directions for the Decade, Snowmass CO, USA, June 25–July 13, 1990, eds. E.L. Berger and R. Craven (World Scientific, 1992) p. 403.

[2] N.V. Mokhov and J.D. Cossairt, Nucl. Instr. and Meth. A 244 (1986) 349;
N.V. Mokhov, Sov. J. Part. and Nuclei (Sept.–Oct. 1987) 408;
N.V. Mokhov, Fermilab Report FN-509 (20 March 1989).

[3] D.E. Groom (ed.), Radiation levels in the SSC interaction regions, SSC Central Design Group Report SSC-SR-1033 (June 1988).

[4] T.A. Gabriel, F.S. Alsmiller, R.G. Alsmiller, Jr., B.L. Bishop, O.W. Hermann and D.E. Groom, SSC Central Design Group Report SSC-110 (1987).

[5] R.G. Alsmiller et al., Nucl. Instr. and Meth. A 313 (1992) 357.

[6] R.G. Alsmiller, Jr., F.S. Alsmiller and O.W. Hermann, Nucl. Instr. and Meth. A 295 (1990) 337;
F.S. Alsmiller and R.G. Alsmiller, Jr., Nucl. Instr. and Meth. A 278 (1989) 713.

[7] T. Handler, P.K. Job, L.E. Price and T.A. Gabriel, Solenoidal Detector Collaboration Note SDC-92-257 (1992);
B.R. Moore, UMS/HEP/91/016 (1992);
T.A. Gabriel, B.L. Bishop, F.S. Alsmiller, R.G. Alsmiller, Jr. and J.O. Johnson, ORNL/TM-11185 (1993).

[8] G. Drews et al., Nucl. Instr. and Meth. A 290 (1990) 335.

[9] J.S. Russ, G.R. Stevenson, A. Fassò, M.C. Nielsen, C. Furetta, P.G. Rancoita and L. Vismara, CERN/TIS-RP/89-02 (1989);

A. Fassò, G.R. Stevenson, M. Bruzzi, C. Furetta, P.G. Rancoita, P. Giubellino, R. Steni and J.S. Russ, CERN/TIS-RP/90-19 (1990);
G.R. Stevenson, A. Fassò, C. Furetta, P.G. Rancoita, P. Giubellino, J.S. Russ and C. Bertrand, CERN/TIS-RP/91-11 (1991).
[10] A. Fassò, A. Ferrari, J. Ranft, P.R. Sala, G.R. Stevenson and J.M. Zazula, in: Proc. Workshop on Simulating Accelerator Radiation Environments, Santa Fe, NM, USA, 11–15 January 1993, eds. L. Waters and A.P.T. Palounek (to be published).
[11] C. Leroy, Y. Sirios and R. Wigmans, Nucl. Instr. and Meth. A 252 (1986) 4.
[12] G.R. Stevenson, CERN/TIS-RP/90-18/CF; also published in: Proc. ECFA Large Hadron Collider Workshop, Aachen, 4–9 October 1990, CERN 90-10, vol. III (1990) p. 302.
[13] M. Höfert and A. Bonifas, CERN/TIS-RP/90-10/CD (1990).
[14] A.E. Brenner et al., Phys. Rev. D 26 (1982) 1497.
[15] D.E. Groom, in: Proc. II Int. Conf. on Calorimetry in High Energy Physics, Capri, Italy, 14–18 October 1991, ed. A. Ereditato (World Scientific,1992) p. 376.
[16] D.E. Groom, in: Proc. Workshop on Calorimetry for the Superconducting Super Collider, Tuscaloosa, AL, USA, 13–17 March 1989, eds. R. Donaldson and M.G.D. Gilchriese (World Scientific,1990) p. 59.
[17] P.A. Aarnio, A. Fassò, H.-J. Möhring, J. Ranft and G.R. Stevenson, CERN/TIS-RP/168 (1986);
P.A. Aarnio, A. Fassò, J. Lindgren, J. Ranft and G.R. Stevenson, CERN/TIS-RP/190 (1987).
[18] F. Pauss et al., Z. Phys. C 27 (1985) 211.
[19] D.E. Groom, Solenoidal Detector Collaboration Note SDC-93-559 (1993).
[20] B.J. Moyer, in: Conf. on Shielding of High-Energy Accelerators, New York, USA, April 11–13 (1957), Oak Ridge National Laboratory Technical Information Service Extension Report TID-7545 (December 1957) p. 96.
[21] K. O'Brien, private communication (1993). For a complete transcript of O'Brien's statement, see K. O'Brien and D.E. Groom, Solenoidal Detector Collaboration Note SDC-93-585 (1993).
[22] K. O'Brien, Health and Safety Laboratory Report HASL-199, U.S. Atomic Energy Commission (1968).
[23] A. Van Ginneken and M. Awschalom, High Energy Particle Interactions in Large Targets. vol. 1, Hadronic Cascades, Shielding, Energy Deposition (Fermilab,Batavia,IL,USA,1975).
[24] T.A. Gabriel and R.T. Santoro, Nucl. Instr. and Meth. 95 (1971) 275.
[25] R.H. Thomas and G.R. Stevenson, Technical Report Series No. 283, IAEA Vienna (1988).
[26] S.J. Lindenbaum, Ann. Rev. Nucl. Sci. 11 (1961) 213.
[27] R.H. Thomas and S.V. Thomas, Health Phys. 46 (1984) 954.
[28] J.D. Cossairt, S.W. Butala and M.A. Gerardi, Nucl. Instr. and Meth. A 238 (1985) 504.
[29] G.R. Stevenson, CERN/TIS/IR/86-04 (1986).
[30] A. Van Ginneken, Fermilab Report FN-272, Fermilab, Batavia, IL, USA (1975).
[31] K. O'Brien, Nucl. Instr. and Meth. 101 (1972) 551.
[32] K. O'Brien, private communication (1989). For a complete transcript of O'Brien's statement, see K. O'Brien and D.E. Groom, Solenoidal Detector Collaboration Note SDC-93-585 (1993).